



# Quantum Circuit Realization of Morphological Gradient for Quantum Grayscale Image

Ping Fan<sup>1</sup> · Ri-Gui Zhou<sup>2</sup> · WenWen Hu<sup>2</sup> · Naihuan Jing<sup>3</sup>

Received: 9 July 2018 / Accepted: 26 October 2018 / Published online: 16 November 2018  
© Springer Science+Business Media, LLC, part of Springer Nature 2018

## Abstract

In this paper, based on the principle of classical morphology operations, the flat grayscale dilation and erosion operations are proposed for NEQR quantum image model. Furthermore, through combining these two morphology operations, we further realize the morphological gradient operation. As the basis of designing of grayscale morphology operations, a series of quantum circuit designs are presented, which includes special add one operation  $UA_1(n)$  and special subtract one operation  $US_1(n)$  both for an  $n$ -length qubits sequence, quantum unitary operation  $U_C$ , parallel subtractor (PS) module, quantum comparator output the large QCOL and quantum comparator output the small QCOS modules. When designing the concrete quantum circuit, a sequence of  $UA_1(n)$  and  $US_1(n)$  modules are used to obtain the quantum image sets based on the shape of specific structuring element. Then, the searching for maxima or minima in a certain space is involved, which can be solved by cascading a series of QCOL and QCOS modules in certain order. Finally, the PS module can be used to calculate the difference of the maxima and minima for producing the morphological gradient. The circuit's complexity analysis illustrates that our scheme is very lower to the classical morphology operations.

**Keywords** Quantum morphological gradient · Quantum dilation · Quantum erosion · Quantum circuit

## 1 Introduction

As the advantages of quantum physics, the idea to simulate physics with computers is put forward [1]. Quantum image processing (QIP) is a young emerging cross-discipline of image processing and quantum mechanics. From 1996, QIP gradually comes into our sight. It is primarily devoted to

---

✉ Ping Fan  
fp\_ecjtu@126.com

<sup>1</sup> School of Information Engineering, East China Jiaotong University, Nanchang 330013 Jiangxi, China

<sup>2</sup> College of Information Engineering, Shanghai Maritime University, Shanghai 201306, China

<sup>3</sup> Department of mathematics, North Carolina State University, Raleigh, NC 27695, USA

utilizing quantum computing technologies to capture, manipulate, and recover quantum images in different formats and for different purposes [2, 3]. Reference [4] describes the “analogue” quantum computers to discuss image analysis. Besides, references [5, 6] design algorithms based on unstructured picture (data set). Due to some of the astounding properties inherent to quantum computation, the quantum computer has demonstrated a bright prospect over the classic computer, particularly in Feynman’s computation model [1], Deutsch’s quantum parallelism assertion [7], Shor’s integer factoring algorithm [8] and Grover’s database searching algorithm [9].

In terms of applications, available literature on quantum image processing can be broadly classified into two groups: quantum-inspired image processing and classically inspired quantum image processing [10–12], respectively. The first step of quantum image processing that is to store images in a quantum computer through quantum image representation. Consequently, several representative models are developed and the pioneering work is the quantum image model of Qubit Lattice [13]. Following that, entangled images, in which geometric shapes are encoded in quantum states [14]; and Real Ket, where the images are quantum states having gray levels as coefficients of the states [15], were proposed by Venegas-Andraca and Latorre, respectively. More recently, Le et al. [16] proposed a flexible representation of quantum image (FRQI) using quantum superposition state to store the colors and the corresponding positions of an image. Years later, more quantum image representations [17–20] were proposed, which includes: a novel enhanced quantum representation (NEQR) [17] used  $q$  qubits encoding the gray-scale values. Thus make the NEQR could perform the complex and elaborate color operations more conveniently than FRQI.

Then, based on the work of quantum image representation models, there are many quantum image processing algorithms, in which includes quantum image geometric transformation [21–24]; quantum image scaling [25–29]; quantum image scrambling [30–32]; quantum image watermarking [33–37]; quantum image steganography based on least significant bit (LSB) [38, 39]; quantum image morphological operation [40–42]; quantum image edge detection [43, 44]; quantum image feature point extraction [45]; quantum image matching [46].

This paper is organized as follows. Section 2 briefly introduces the quantum image model NEQR and the classical morphology operations for the grayscale image. A series of specific quantum circuit are constructed to realize a certain function in Section 3. The specific quantum circuit realization morphological gradient for quantum gray-scale image is proposed. Section 5 analyses the circuit’s complexity and experimental results. The conclusions and future work is drawn in section 5.

## 2 Preliminaries

In this paper, the quantum image NEQR (i.e. a novel enhanced quantum representation of digital images) model is introduced first. Then, the morphology operations for the grayscale image that includes the flat grayscale dilation, erosion and their combination operation of morphology gradient are illustrated in detail.

### 2.1 Quantum Image Model NEQR and Circuit Complexity

#### 2.1.1 The Novel Enhanced Quantum Representation (NEQR)

As for an  $2^n \times 2^n$  image with grayscale range  $[0, 2^q - 1]$ , NEQR uses  $q$  qubits to represent color information and  $2n$  qubits to represent position information. But for a binary image, the color

information just includes two values 0 and 1 (therein  $q = 1$ ). Thus, the gray-scale value  $C_{YX}$  of the pixel coordinate  $(Y, X)$  can be expressed by Eq. (1).

$$C_{YX} = C_{YX}^0 C_{YX}^1 \dots C_{YX}^{q-2} C_{YX}^{q-1}, C_{YX}^k \in \{0, 1\}, C_{YX} \in [0, 2^q - 1] \tag{1}$$

Therefore, the NEQR quantum image representation can be written as Eq. (2) for an  $2^n \times 2^n$  image with grayscale range  $[0, 2^q - 1]$ .

$$|I\rangle = \frac{1}{2^n} \sum_{Y=0}^{2^n-1} \sum_{X=0}^{2^n-1} |C_{YX}\rangle |Y\rangle |X\rangle = \frac{1}{2^n} \sum_{YX=0}^{2^{2n}-1} \bigotimes_{k=0}^{q-1} |C_{YX}^k\rangle |YX\rangle \tag{2}$$

Figure 1 shows an image and the corresponding NEQR state is on the right.

### 2.1.2 Simple Quantum Gates and circuit’s Complexity

**Quantum Gates** In the quantum circuit model, a complex transformation can be broken down into universal quantum logic gates [47], i.e., single-qubit gate, two-qubit and three-qubit gates, such as NOT, Controlled-V gate, Controlled-V<sup>+</sup> gate, Feynman gate (FG) [48], Toffoli gate [49] and Peres gate [50] and Thapliyal Ranganathan gate [51] which are shown in Fig. 2.

Therein, V is a square-root-of NOT gate and V<sup>+</sup> is its Hermitian. Thus, VV or V<sup>+</sup>V<sup>+</sup> creates a unitary matrix of NOT gate and VV<sup>+</sup> = V<sup>+</sup>V = I (an identity matrix), which can be described as Eq. (3).

$$\begin{aligned} V \times V &= V^+ \times V^+ = X \\ V \times V^+ &= V^+ \times V = I \end{aligned} \tag{3}$$

As shown in Fig. 2, the FG can accomplish XOR function. It is easy to conclude that when cascades (n-1) FG gates we can realize n-bit XOR operation. The concrete quantum circuit realization and corresponding block diagram are shown in Fig. 3.

**Quantum circuit’s Complexity** In the quantum circuit model, a complex transformation can be broken down into simpler gates, i.e., single-qubit gate, two-qubit and three-qubit gates. Therefore, the circuit complexity of any single-qubit gate, two-qubit and three-qubit gates are taken as unity. The circuit’s complexity is determined by the number of these simpler gates. Based on this principle, it is obvious that the NOT gate, FG, Controlled-V gate, Controlled-V<sup>+</sup> gate and TG can take as unity 1. The PG is composed by 2 Controlled-V gates, 1 Controlled-V<sup>+</sup> gate and 1 FG, therefore, the circuit complexity of PG is 4. As shown in Fig. 3, the n-bit XOR operation is constructed by cascading (n-1) FG, thus the circuit complexity of n-bit XOR module is (n-1).

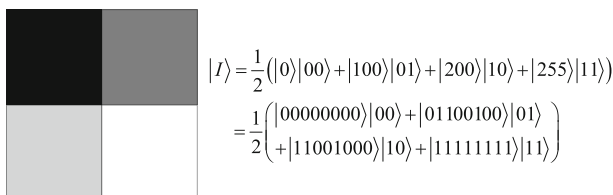


Fig. 1 An  $2 \times 2$  NEQR image and its quantum state is on the right

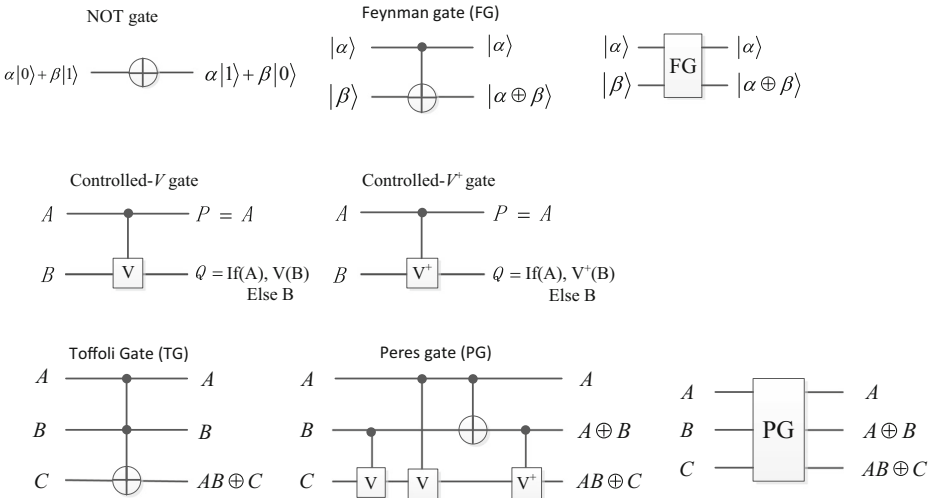


Fig. 2 Some single-qubit gate, two-qubit and three-qubit gates

### 2.2 Classical Grayscale Morphology Operations

The grayscale morphology is built on binary morphological. In this section, we focus on flat grayscale quantum dilation and erosion operations which are defined in terms of minima and maxima of pixel neighborhoods [52]. Then, based on the flat grayscale dilation and erosion operations, we further introduce the conception of morphological gradient.

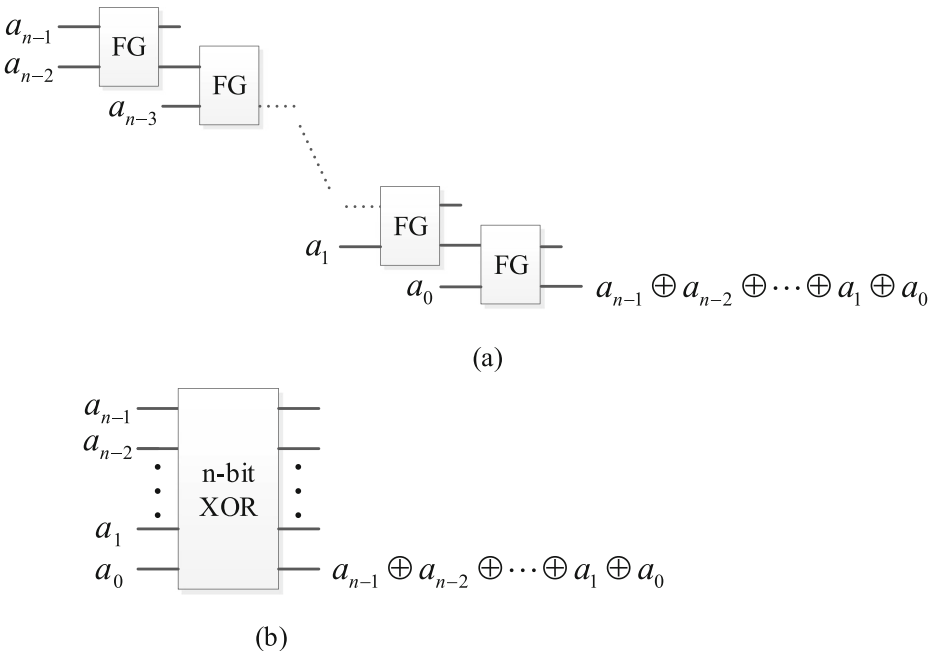


Fig. 3 a The quantum circuit realization of n-bit XOR operation, b the block diagram of n-bit XOR operation

### 2.2.1 The Classical Flat Grayscale Dilation Operation

A function is used to represent the grayscale dilation operation of image  $F$  by structuring element  $B$  as denoted by

$$(F \oplus B)(s, t) = \max\{F(s-x, t-y) | (x, y) \in D_B\} \tag{4}$$

where  $D_B$  is the domain of  $b$  and  $F(x, y)$  is assumed to equal  $-\infty$  outside the domain of  $F$ .

Actually, the grayscale dilation operation always done by the flat structuring element, in which means that the value of  $B$  is 0 at all coordinates over  $D_B$  definition. That is,

$$B(x, y) = 0, (x, y) \in D_B \tag{5}$$

In this case, the max operation is specified completely by the value of 0 and 1 in binary matrix  $D_B$ , and the grayscale dilation equation is simplified to

$$(F \oplus B)(s, t) = \max\{F(s-x, t-y) | (x, y) \in D_B\} \tag{6}$$

Thus, flat grayscale dilations are a local-maximum operator, where the maximum is taken over a set of pixel neighbors determined by the shape of  $D_B$ .

An example, as shown in Fig. 4, illustrates that the flat grayscale dilation is a local-maximum operator.

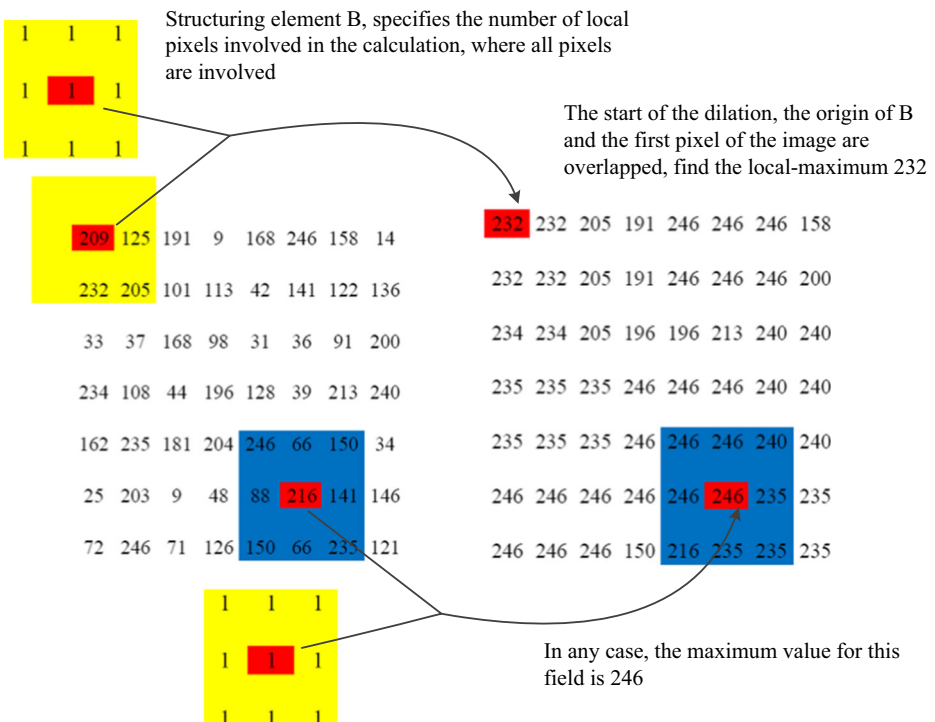


Fig. 4 The flat grayscale dilation is a local-maximum operator

### 2.2.2 The Classical Grayscale Erosion Operation

A function is used to represent the grayscale erosion operation of image F by structuring element B as denoted by

$$(F \ominus B)(s, t) = \min\{F(s + x, t + y) - B(x, y) | (x, y) \in D_B\} \tag{7}$$

where  $D_B$  is the domain of b and  $F(x, y)$  is assumed to equal  $+\infty$  outside the domain of F.

Conceptually, we again can think of translating the structuring element to all locations in the image. At each translated location, the structuring element values are subtracted to the image pixel values and the minimum is computed.

As with dilation, grayscale erosion is most often performed using flat structuring elements. The equation for flat grayscale erosion can then be simplified to

$$(F \ominus B)(s, t) = \min\{F(s + x, t + y) | (x, y) \in D_B\} \tag{8}$$

Thus, flat grayscale erosion is a local-minimum operator, in which the minimum is taken over a set of pixel neighbors determined by the shape of  $D_B$ . So, the erosion problem transfers to search for minimum.

An example, shown in Fig. 5, illustrates that the flat grayscale erosion is a local-minimum operator.

### 2.2.3 The Classical Morphological Gradient for Grayscale Image

Dilation and erosion can be used in combination, subtracting the eroded image from the dilated image can produce a morphological gradient, which is a measure of the local gray level change in the image. Thus, the function of morphological gradient based on the flat element can be written as follows.

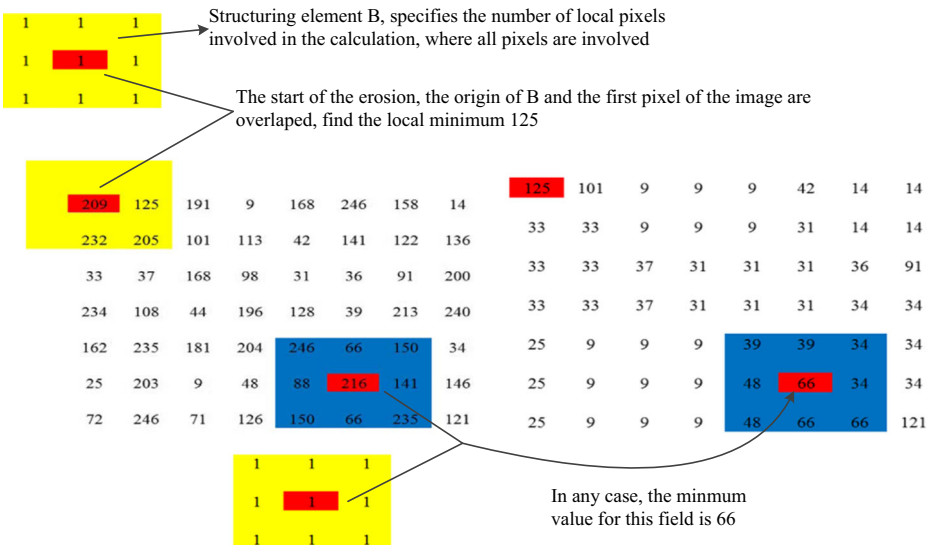


Fig. 5 The flat grayscale erosion is a local-minimum operator

$$MF = (F \oplus B)(s, t) - (F \ominus B)(s, t) = [\max\{F(s + x, t + y)\} - \min\{F(s - x, t - y)\}], (x, y) \in D_B \tag{9}$$

### 3 Quantum Circuit Design

In this section, a series of specific quantum circuit are designed to realize a certain function, which includes special add one operation  $UA_1(n)$ , special subtract one operation  $US_1(n)$ , quantum unitary operator  $U_C$  and the parallel full subtractor PS. All of the mentioned quantum circuit will be used in the proposed morphology operations.

#### 3.1 Special Add One Operation

The quantum circuit realization of special add one operation  $UA_1(n)$  for an  $n$ -length qubits sequence is shown in Fig. 6. When  $UA_1(n)$  works on the  $n$  qubits quantum state  $|x_{n-1}x_{n-2} \cdots x_1x_0\rangle$  (Input), the result (Output) will be the  $|x_{n-1}x_{n-2} \cdots x_1x_0 + 1\rangle$  if and only if  $x_{n-1} \times x_{n-2} \times \cdots \times x_1 \times x_0 \neq 1$ . Otherwise, the  $n$  qubits quantum state  $|x_{n-1}x_{n-2} \cdots x_1x_0\rangle$  will not be changed. The function of  $UA_1(n)$  can be expressed by Eq. (10).

$$UA_1(n)|x_{n-1} \cdots x_1x_0\rangle = \begin{cases} |x_{n-1} \cdots x_1x_0 + 1\rangle, & x_{n-1} \times x_{n-2} \times \cdots \times x_1 \times x_0 \neq 1 \\ |x_{n-1} \cdots x_1x_0\rangle, & x_{n-1} \times x_{n-2} \times \cdots \times x_1 \times x_0 = 1 \end{cases} \tag{10}$$

therein,  $n$  is a positive natural number,  $n \geq 2$ ,  $x_0, x_1, \dots, x_{n-1} \in \{0, 1\}$ .

#### 3.2 Special Subtract One Operation

The quantum circuit realization of special subtract one operation  $US_1(n)$  for an  $n$ -length qubits sequence is shown in Fig. 7. When  $US_1(n)$  works on the  $n$  qubits

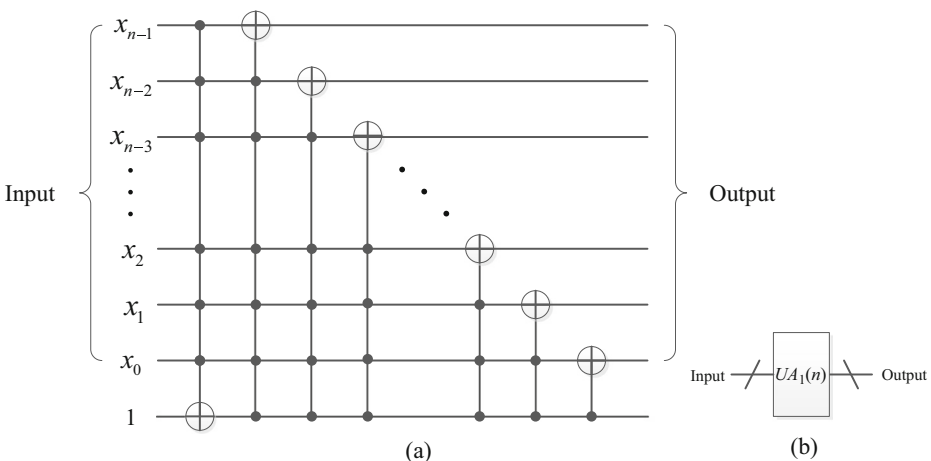


Fig. 6 a Quantum circuit realizations of  $UA_1(n)$ , b the block diagram of  $UA_1(n)$

quantum state  $|x_{n-1}x_{n-2}\cdots x_1x_0\rangle$  (Input), the result (Output) will be the  $|x_{n-1}x_{n-2}\cdots x_1x_0-1\rangle$  if and only if  $x_{n-1} \times x_{n-2} \times \cdots \times x_1 \times x_0 \neq 0$ . Otherwise, the  $n$  qubits quantum state  $|x_{n-1}x_{n-2}\cdots x_1x_0\rangle$  will not be changed. The function of  $US_1(n)$  can be expressed by Eq. (11).

$$US_1(n)|x_{n-1}x_{n-2}\cdots x_1x_0\rangle = \begin{cases} |x_{n-1}x_{n-2}\cdots x_1x_0-1\rangle, & x_{n-1} \times x_{n-2} \times \cdots \times x_1 \times x_0 \neq 0 \\ |x_{n-1}x_{n-2}\cdots x_1x_0\rangle, & x_{n-1} \times x_{n-2} \times \cdots \times x_1 \times x_0 = 0 \end{cases} \quad (11)$$

therein,  $n$  is a positive natural number,  $n \geq 2$ ,  $x_{n-1}x_{n-2}\cdots x_1x_0 \in \{0, 1\}$ .

### 3.3 Quantum Unitary Operation $U_C$

The quantum unitary operation  $U_C$  as defined in Eq. (12) can copy the  $q$ -length qubit sequence information of  $|C\rangle = |c_{q-1}c_{q-2}\cdots c_0\rangle$  into the  $q$  ancillary qubits  $|0\rangle^{\otimes q}$ . The quantum circuit realization of  $U_C$  is shown in Fig. 8.

$$U_C(|C\rangle|0\rangle^{\otimes n}) = |C_{YX}\rangle|C_{YX}\rangle \quad (12)$$

### 3.4 Quantum Comparator Circuit

In this section, the  $n$ -bit reversible comparator is designed through the 1-bit reversible comparator, in which a series of basic quantum gates (NOT, CNOT, PG and Toffoli gate) are used to construct the synthetic circuit.

#### 3.4.1 1-Bit Reversible Comparator

The result of 1-bit compares shown in Table 1. From the truth table of connectional comparator in Table 1, the logical expressions of 1-bit comparator is as follows:

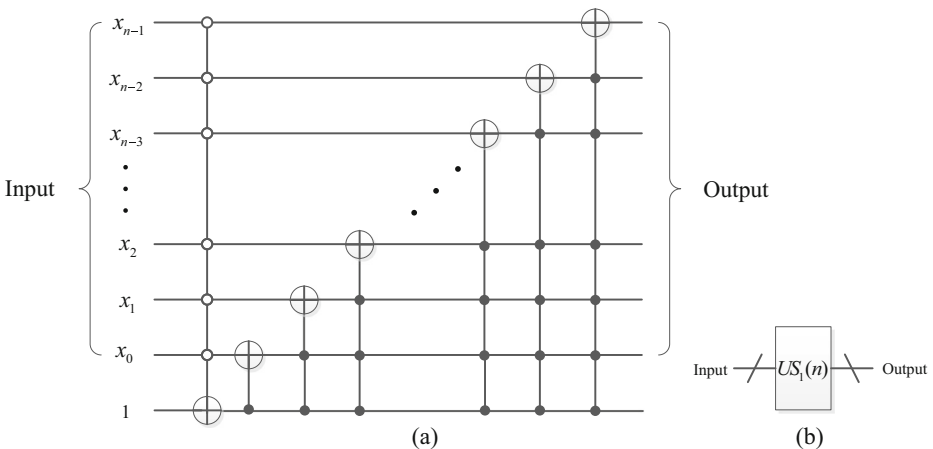


Fig. 7 a Quantum circuit realizations of  $US_1(n)$ , b the block diagram of  $US_1(n)$



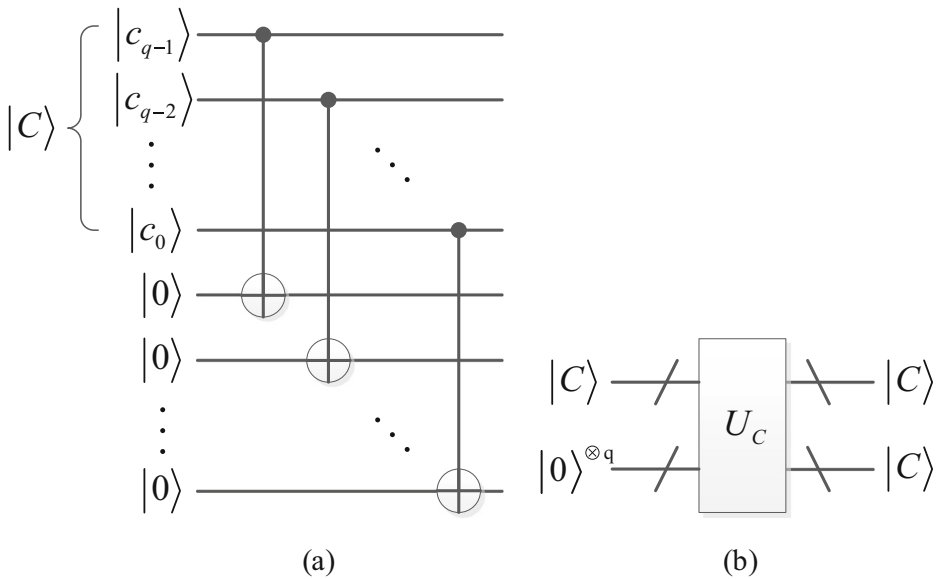


Fig. 8 a Quantum circuit for unitary operation  $U_C$ , b the simplified graph of  $U_C$

$$\begin{aligned}
 F_{A>B} &= A\bar{B} \\
 F_{A=B} &= A\oplus B \\
 F_{A<B} &= \bar{A}B
 \end{aligned}
 \tag{13}$$

According to the logical expression of Eq. (13), the quantum circuit realization 1-bit reversible comparator as illustrated in Fig. 9.

The conventional n-bit comparator is used for comparing two n-bit numbers like  $A = a_{q-1}a_{q-2}\dots a_1a_0$  and  $B = b_{q-1}b_{q-2}\dots b_1b_0$ . The logical expression of n-bit comparator can be written as Eq. (14).

$$\begin{aligned}
 F_{A>B} &= (a_{q-1} > b_{q-1}) \oplus (a_{q-1} = b_{q-1})(a_{q-2} > b_{q-2}) \oplus \dots \\
 &\quad \oplus (a_{q-1} = b_{q-1})(a_{q-2} = b_{q-2}) \dots (a_2 = b_2)(a_1 = b_1)(a_0 > b_0) \\
 F_{A=B} &= (a_{q-1} = b_{q-1})(a_{q-2} = b_{q-2}) \oplus \dots \oplus (a_1 = b_1)(a_0 = b_0) \\
 F_{A<B} &= (a_{q-1} < b_{q-1}) \oplus (a_{q-1} = b_{q-1})(a_{q-2} < b_{q-2}) \oplus \dots \\
 &\quad \oplus (a_{q-1} = b_{q-1})(a_{q-2} = b_{q-2}) \dots (a_2 = b_2)(a_1 = b_1)(a_0 < b_0)
 \end{aligned}
 \tag{14}$$

According to logical expression of q-bit conventional binary comparator, equation of  $F_{A<B}$  also can be obtained as followed:

Table 1 The truth table of 1-bit comparator

Input		Output		
A	B	$F_{A>B}$	$F_{A=B}$	$F_{A<B}$
0	0	0	1	0
0	1	0	0	1
1	0	1	0	0
1	1	0	1	0

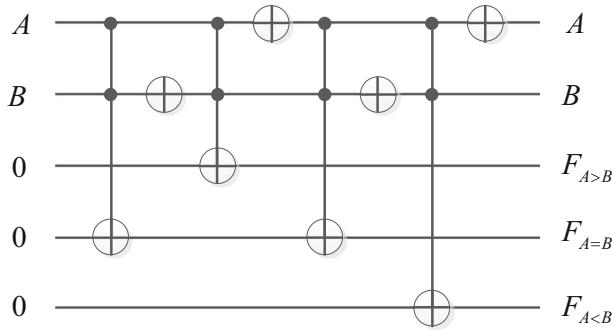


Fig. 9 Quantum circuit realization of 1-bit reversible comparator

$$F_{A<B} = \overline{F_{A>B} \oplus F_{A=B}} \tag{15}$$

Combine the principle illustrated in Eq. (14) and Eq. (15) that the comparative results of  $F_{A<B}$  for q-bit A and B can be deduced from the corresponding results of  $F_{A>B}$  and  $F_{A=B}$ . Thus, the basic quantum comparator for 1-bit module (QC1) that deduces from the 1-bit reversible comparator can be rebuilt as illustrated in Fig. 10, which would be used to build the integrate quantum comparator and output the large and small circuits for q-bit in latter.

### 3.4.2 Q-Bit Reversible Comparator and Output the Large

Combine the logical value described in Eq. (14) and Eq. (15), the circuit realization of q-bit reversible comparator and output the large (QCOL) is constructed through the QC1 module, n-bit xor gate, PG gate and FG gate, as shown in Fig. 11.

### 3.4.3 Q-Bit Reversible Comparator and Output the Small

Similar to quantum circuit for QCOL, the circuit realization of q-bit reversible comparator and output the small (QCOS) is constructed through the QC1 module, n-bit xor gate, PG gate and FG gate, as shown in Fig. 12.

For convenience, Fig. 13 gives the simplified block diagram QCOL and QCOS modules, which omits the constant inputs and garbage outputs.

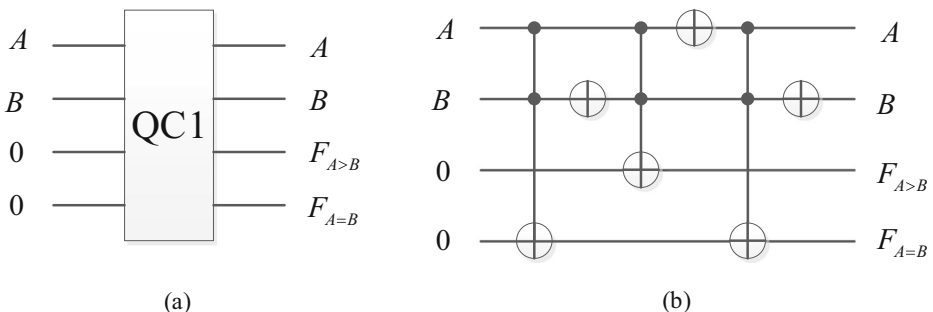


Fig. 10 a The QC1 module, b quantum circuit for the QC1 module

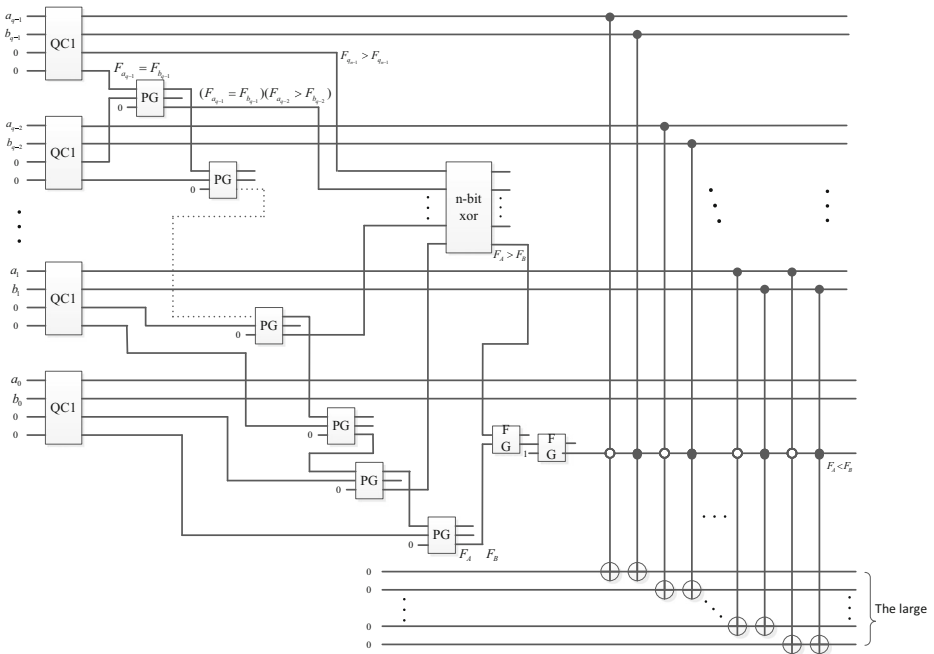


Fig. 11 q-bit reversible comparator and output the large

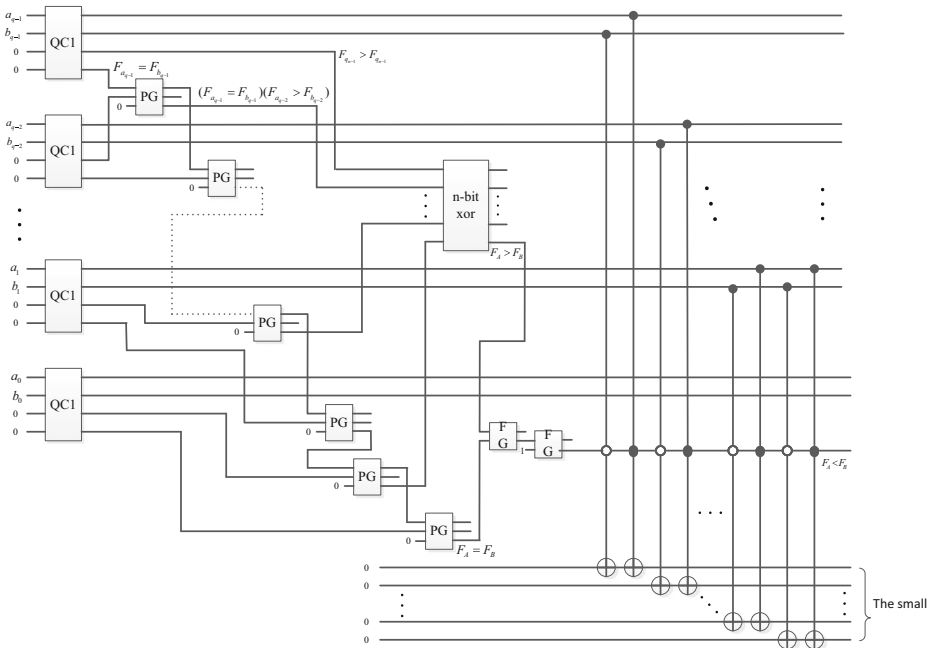
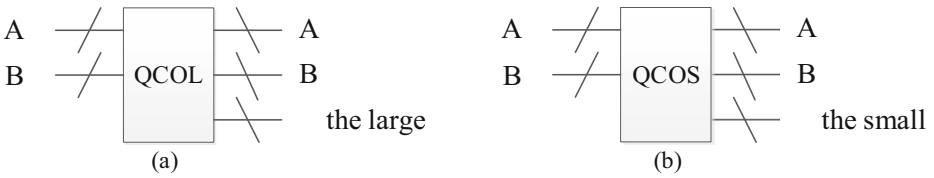


Fig. 12 q-bit reversible comparator and output the small



**Fig. 13** **a** The block diagram of QCOL, **b** the block diagram of QCOS

As shown in Fig. 13,  $A = a_{q-1}a_{q-2} \dots a_1a_0$  and  $B = b_{q-1}b_{q-2} \dots b_1b_0$ . In QCOL module, if  $A \geq B$ , the large = A; Otherwise, the large = B. In QCOS module, if  $A \geq B$ , the small = B; Otherwise, the small = A.

**3.5 The Parallel Subtractor (PS) Circuit**

Thapliyal H. and Ranganathan N. [51] designed subtractor using the TR gate and further realized optimization in terms of quantum cost and delay in [53]. Here, the concrete design of parallel subtractor circuit is given.

(a) Reversible half subtractor (RHS)

The RHS can be used to calculate two 1-bit numbers difference, where the corresponding truth value of RHS is shown in Table 2. Therein, the inputs of  $a_0$  and  $b_0$  are 1-bit binary number while  $d_0$  and  $b_0$  denote the corresponding difference and borrow of  $b_0 - a_0$ , respectively. The simplified graph of RHS module and its quantum circuit realization are illustrated in Fig. 14, where  $|a_0 \oplus b_0\rangle$  represents the difference of  $|b_0 - a_0\rangle$ , and  $|a_0 \bar{b}_0\rangle$  generates the corresponding borrow bit.

(b) Reversible fullsubtractor (RFS)

The RFS can be used to calculate three 1-bit numbers difference, where the corresponding truth value of RFS is shown in Table 3. Therein, the inputs of  $a_0, b_0$  and  $c_0$  are 1-bit binary number while  $d_0$  and  $b_0$  denote the corresponding difference and borrow of  $a_0 - b_0 - c_0$ , respectively. The simplified graph of RFS module and its quantum circuit realization are illustrated in Fig. 15, where  $|a_0 \oplus b_0 \oplus c_0\rangle$  represents the difference of  $|a_0 - b_0 - c_0\rangle$ , and  $a_0(b_0 \oplus c_0) \oplus b_0 \bar{c}_0$  generates the corresponding borrow bit.

(c) Parallel subtractor (PS)

The parallel subtractor (PS) is used to compute the difference of two  $n$ -bit numbers  $X$  and  $Y$ , wherein  $X = x_{n-1} \dots x_0$ ,  $Y = y_{n-1} \dots y_0$ . Assume that we define the difference of  $X - Y$  is  $d_n d_{n-1} \dots d_1 d_0$ . Because of the highest bit  $d_n$  is a sign bit, i.e., if  $d_n = 1$ , then  $X < Y$ ; otherwise,  $d_n = 0$  and  $X \geq Y$ . The PS module are designed using 1 RHS and  $(n-1)$  RFS as shown in Fig. 16(a). For

**Table 2** The truth table of RHS

$a_0$	$b_0$	$d_0$	$b_0$
0	0	0	0
0	1	1	0
1	0	1	1
1	1	0	0

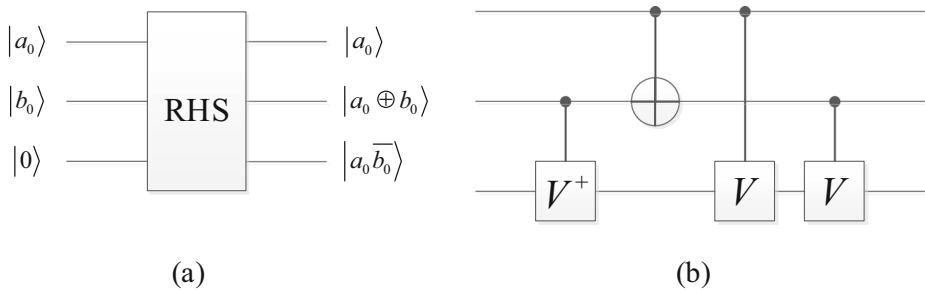


Fig. 14 a The block diagram of RHS module, b quantum circuit realization of RHS module

convenience, the block diagram of PS omits the constant ancillary bit 0 and the other unmarked garbage outputs as shown in Fig. 16(b).

### 4 Circuit Realization Morphological Gradient for Quantum Gray-Scale Image

In this section, the quantum circuit for quantum gray-scale image dilation and erosion are constructed first. Then, based on the results of quantum dilation and erosion, the quantum morphological gradient operation is done through the PS module, which subtracts the eroded image from the dilated image. Finally, through the quantum measurement, the classical morphological gradient can be obtained.

#### 4.1 Workflow of Quantum Grayscale Image Morphological Gradient Operation

The whole procedure of quantum morphological gradient operation is shown in Fig. 17, which is divided into many steps more specifically.

Here, the working principle of the whole procedure is introduced briefly. The first step in this whole procedure is to quantize the classical image into a quantum image based on NEQR expression model. Following that, A series of modules  $UA_1(n)$  and  $US_1(n)$  are implemented in a certain order to shift the quantum image based on the specific shape of structuring element and the quantum unitary operation  $U_C$  modules to copy the corresponding the pixel information of the shifted quantum image into prepared extra ancillary qubit sequences. Thus, we can obtain the quantum image sets, which is associated with the specific shape of the structuring element. And now, based on these quantum image sets, the QCOL modules is used to find the local-maximum (the quantum dilation result) and the QCOS modules is used to find the local-minimum (the

Table 3 The truth table of RFS

$a_0$	$b_0$	$c_0$	$d_0$	$b_0$
0	0	0	0	0
0	0	1	1	1
0	1	0	1	1
0	1	1	0	1
1	0	0	1	0
1	0	1	0	0
1	1	0	0	0
1	1	1	1	1

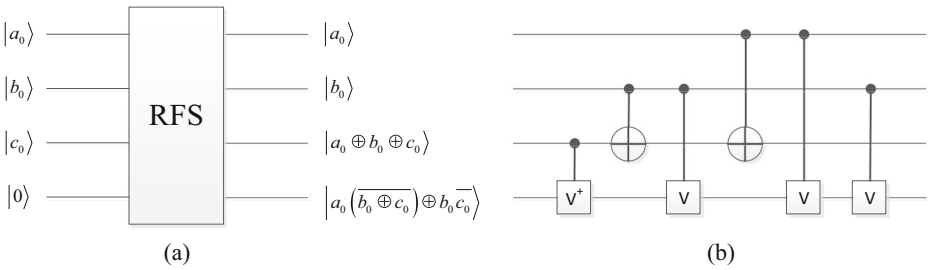


**Fig. 15** **a** The simplified graph of RFS module, **b** quantum circuit for RFS module

quantum erosion result), respectively. Finally, the quantum morphological gradient can be obtained by subtracting the eroded image from the dilated image through PS module.

**4.2 Quantum Circuit Realization Quantum Dilation and Erosion Operations**

Suppose that there adigital image is quantized into a NEQR quantum image with size  $2^n \times 2^n$  and gray range  $[0, 2^q - 1]$ , which is expressed by Eq. (2). The flat structuring element B as shown in Fig. 18 is a  $3 \times 3$ -mtric including 9 neighbor pixels.

Through the analysis of classical grayscale morphology operations in subsection 2.2.1 and 2.2.2, it is easy to find that the result of the flat grayscale image dilation and erosion are the local-maximum and local minimum operators, respectively. Therein, the maximum and minimum values are taken over a set of neighbor pixels determined by the exact shape of structuring element. Based on this principle, the integrated quantum circuit design is divided into two steps as shown in Fig. 19 and Fig. 20.

Step 1. Firstly, prepare the eight extra qubits  $|0\rangle^{\otimes 8q}$  sequences as defined in Eq. (16), which is in a tensor product with the original quantum image state. Then, implement the

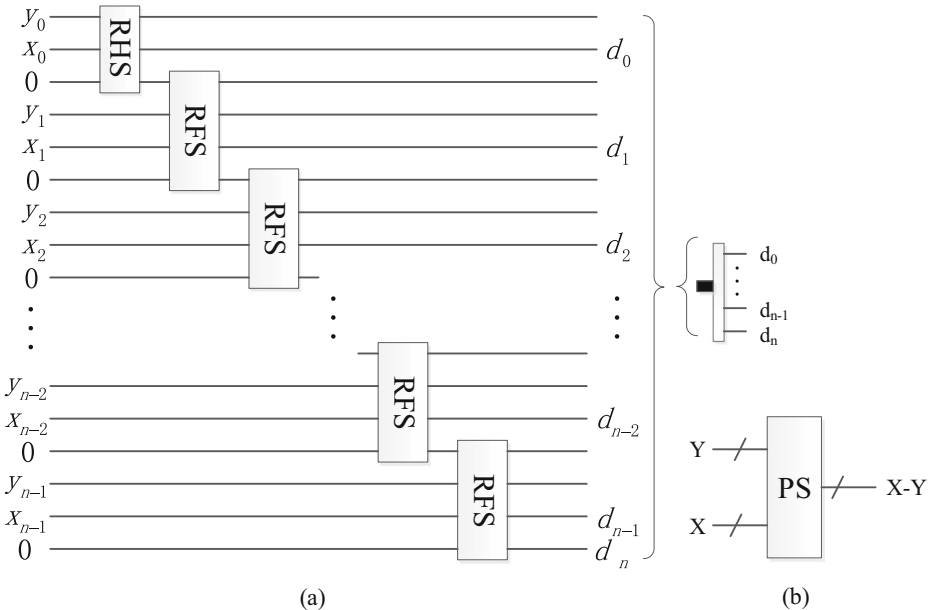


**Fig. 16** **a** quantum circuit realization of PS module, **b** thesimplified graph of PS module

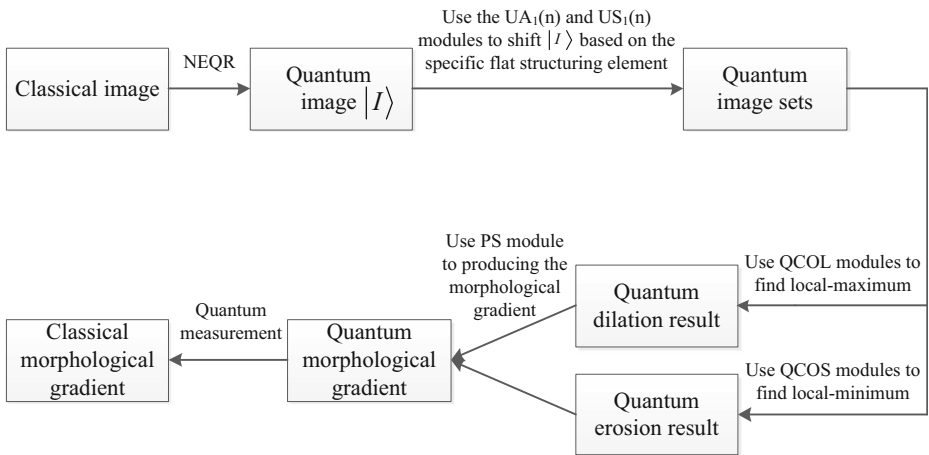


Fig. 17 Whole procedure of quantum morphological gradient operation

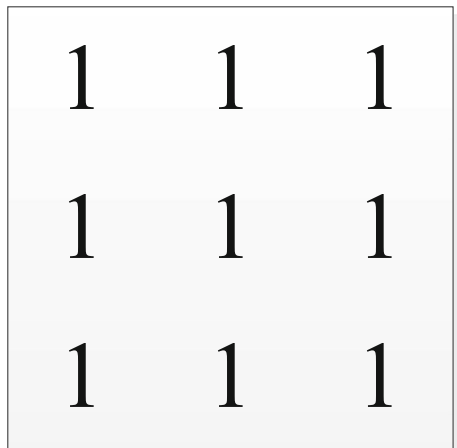
special add one operation  $UA_1(n)$ , special subtract one operation  $US_1(n)$  and quantum unitary operation  $U_C$  in a certain order on the original quantum image, we can get the 9 qubits information of the neighbor pixels of the whole image and store them into the prepared qubit sequences. The concrete circuit realization of this step is shown in Fig. 19.

$$\frac{1}{2^n} \sum_{Y=0}^{2^n-1} \sum_{X=0}^{2^n-1} |0\rangle^{\otimes 8q} |C_{YX}\rangle |Y\rangle |X\rangle = \frac{1}{2^n} \sum_{YX=0}^{2^{2n}-1} |0\rangle^{\otimes 8q} \otimes_{k=0}^{q-1} |C_{YX}^k\rangle |YX\rangle \quad (16)$$

Therefore, we can get therelative color qubits of the neighbor pixels of the whole image, i.e., the quantum image sets where all the pixels share the same position state as defined in Eq. (17).

$$\frac{1}{2^n} \sum_{Y=0}^{2^n-1} \sum_{X=0}^{2^n-1} |C_{YX}\rangle |C_{Y-1X}\rangle |C_{Y-1X+1}\rangle |C_{YX+1}\rangle |C_{Y+1X+1}\rangle |C_{Y+1X}\rangle |C_{Y+1X-1}\rangle |C_{YX-1}\rangle |C_{Y-1X-1}\rangle |Y\rangle |X\rangle \quad (17)$$

Fig. 18 Structuring element B



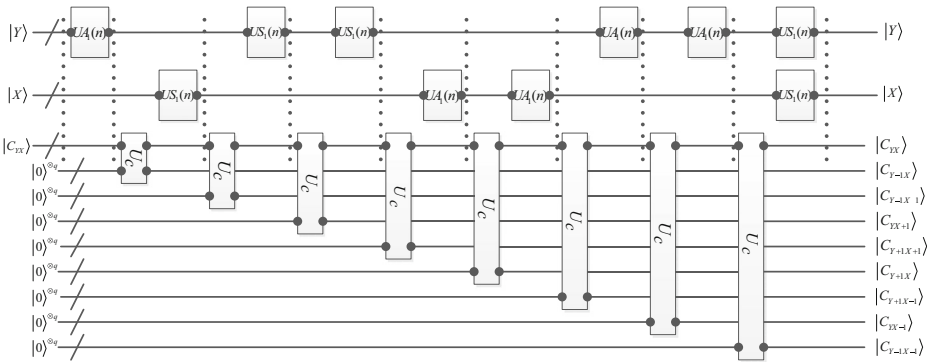


**Fig. 19** Quantum circuit realization obtaining 9 neighbor pixels according to structuring element B

Step 2. Eight QCOL and Eight QCOS modules are cascaded for finding the local-maximum pixel and local-minimum pixel in quantum image sets, respectively. The specific circuit design is shown in Fig. 20.

Therefore, though the above two steps, we can obtain the quantum dilation and erosion results, which can be expressed Eq. (18)

$$|results\rangle = \frac{1}{2^n} \sum_{Y=0}^{2^n-1} \sum_{X=0}^{2^n-1} |D_{YX}\rangle |E_{YX}\rangle |Y\rangle |X\rangle \tag{18}$$

therein, the qubit sequence  $|D_{YX}\rangle$  and  $|E_{YX}\rangle$  are entangled with each other and share the same position coordinates.

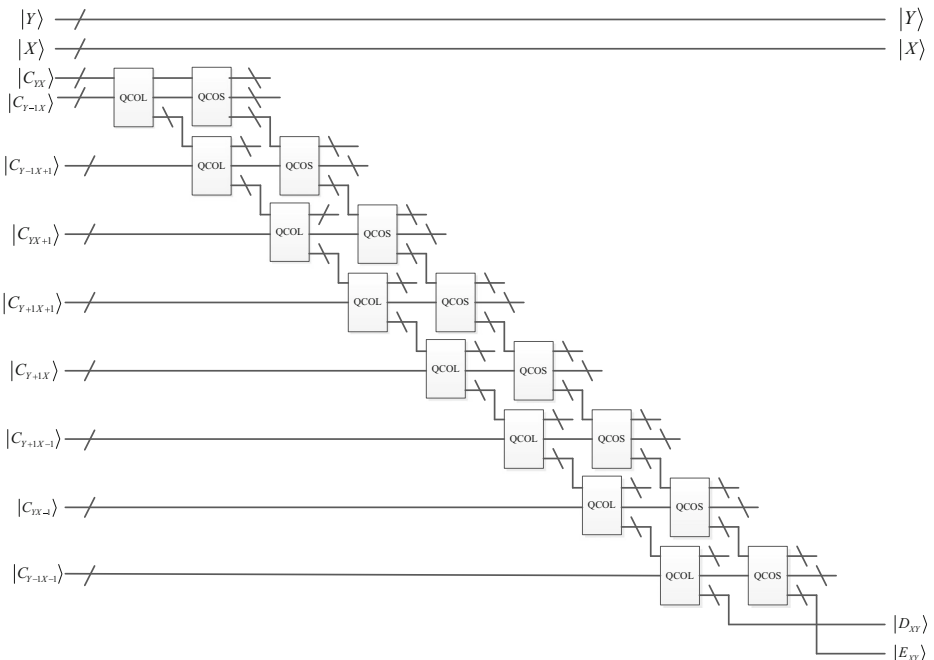


**Fig. 20** Finding the local-maximum and local-minimum in any  $3 \times 3$  neighbor window



### 4.3 Quantum Circuit Realization Quantum Morphological Gradient Operation

According to principle of the classical morphological gradient in subsection 2.2.3, we know that the morphological gradient operation can be done through the dilation and erosion operations. Based on this principle, Fig. 21 provides the concrete quantum circuit realization of the morphological gradient, which a single PS module is used to subtract quantum erosion result  $|E_{YX}\rangle$  from the quantum dilation result  $|D_{YX}\rangle$ .

Thus, we obtain the quantum morphological gradient as Eq. (19)

$$|G\rangle = \frac{1}{2^n} \sum_{Y=0}^{2^n-1} \sum_{X=0}^{2^n-1} |G_{YX}\rangle |Y\rangle |X\rangle \tag{19}$$

## 5 Circuit Complexity and Experiment Analyses

In this section, the circuit complexity of morphological gradient operation for quantum grayscale image discussed firstly, which includes three figures (Fig. 19, Fig. 20 and Fig. 21). Then, the experiment results are simulated based on the classical computer’s MATLAB software.

### 5.1 Circuit Complexity Analysis

Here consider a size of  $2^n \times 2^n$  quantum image with grayscale range  $[0, 2^q - 1]$  as an example. Similarly, the circuit’s complexity analysis is divided into three steps according to the circuit realization three steps.

**Step 1.** The quantum circuit realization as shown in Fig. 19, therein, 5  $UA_1(n)$  modules and 5  $US_1(n)$  modules both are for an  $n$ -length qubits sequence, and 8  $U_C$  modules. The single  $U_C$  module is constructed by  $q$  FG gates (shown in Fig. 8), thus its circuit’s complexity is  $q$ . As shown in Fig. 6 and Fig. 7, the single  $UA_1(n)$  and  $US_1(n)$  module both are comprised by  $(n-1)$  multi-CNOT (which means the circuit’s control qubits not just one) of  $CNOT$ ,  $2 - CNOT \cdots (n - 2) - CNOT$ ,  $(n - 1) - CNOT$  and two  $n - CNOT$ . According to analysis of [44, 54], a  $K$ -CNOT quantum gate (where  $K$  represents the number of control qubits,  $K \geq 3$ ) can be constructed by  $(4K - 8)$  2-CNOT gates (TG) and  $(K - 3)$  assistant qubits. Therefore, the circuit’s complexity of single  $UA_1(n)$  or  $US_1(n)$

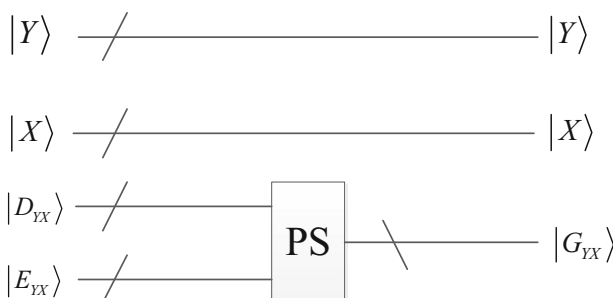
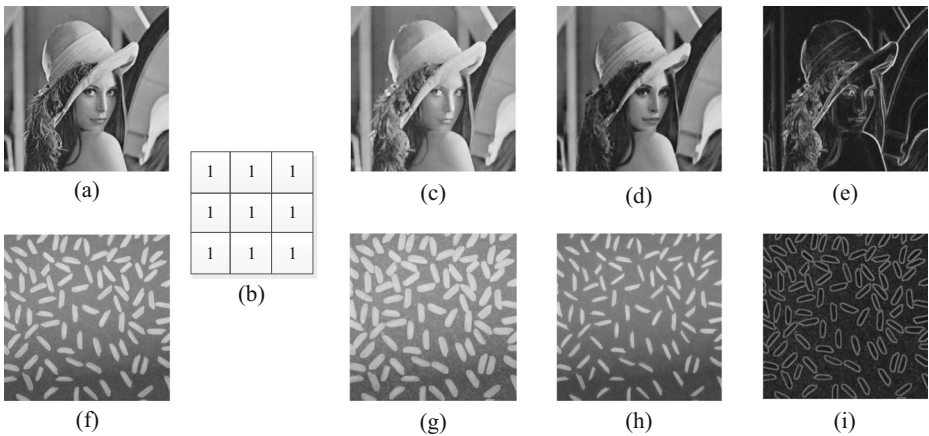


Fig. 21 Subtract the eroded image from the dilated image to produce the morphological gradient



**Fig. 22** (a) grayscale image Lena. (b) flat structuring element B. (c) the flat grayscale dilation of Lena by B. (d) the flat grayscale erosion of Lena by B. (e) the morphological gradient producing by (c) and (d); (f) grayscale image Rice. (g) the flat grayscale dilation of Rice by B. (h) the flat grayscale erosion of rice by B. (i) the morphological gradient producing by (g) and (h)

module is  $1 + \sum_{K=3}^{n-1} (4K-8) + 2(4n-8) = 2n^2 - 2n + 5$ . Thus, the circuit’s complexity in step 1 is  $10 \times (2n^2 - 2n + 5) + 8q = 20n^2 - 20n + 8q + 50$ .

**Step 2.** The quantum circuit realization as shown in Fig. 20, therein, 8QCOL modules and 8 QCOS modules both are for an  $q$ -length qubits sequence. The single QCOL and QCOS modules are shown in Fig. 11 and Fig. 12, respectively, which both are composed by  $q$  QC1 modules,  $2(q-1)$  PG gates, 2 FG gates and  $2q$  2-CNOT gates. Therein, QC1 module is shown in Fig. 10, which circuit’s complexity is 6, and the PG gate and FG gate are shown in Fig. 2 of which circuit’s complexity are 4 and 2, respectively. Thus, we can calculate that the single QCOL or QCOS module is  $6q + 4 \cdot 2(q-1) + 2 + 2q$ . Therefore, the circuit’s complexity in this step is  $16 \times (6q + 4 \cdot 2(q-1) + 2 + 2q) = 256q - 96$ .

**Step 3.** The quantum circuit realization is shown in Fig. 21. Therein, just only one PS module for a  $q$ -length qubits sequence is used to calculate the difference of the local-maximum and local-minimum. Thus the PS module can be constructed by 1 RHS module and  $(q-1)$  RFS module. As shown in Fig. 14 and Fig. 15, single RHS module and single RFS module circuit’s complexity are 4 and 6, respectively. Thus the circuit’s complexity of this step is  $6(q-1) + 4 = 6q - 2$ .

According to the circuit’s complexity analysis in above three steps, we can conclude that the integrated circuit complexity is equal to the sum of the three steps, that is

$$\begin{aligned} & (20n^2 - 20n + 8q + 50) + (256q - 96) + (6q - 2) \\ & = 20n^2 + 270q - 20n - 48 \\ & \approx O(20n^2 + 270q) \end{aligned}$$

For classical dilation and erosion operations, the complexity is  $O(m^2 2^{2n})$  where the size of structuring element and original image are  $m \times m$  and  $2^n \times 2^n$ , respectively. Therefore, our proposed quantum circuit scheme has a very lower complexity to the classical one.

## 5.2 Simulation Analysis

All the experiments are simulated by MATLAB 2014 on the classical computer. Two common test images Lena and Rice were chosen, and the structuring element is a  $3 \times 3$  1-matrix. The experiment results are shown in Fig. 22.

## 6 Conclusions

Morphology provides an approach to the processing of digital images based on shape. In this paper, quantum implementation circuits of flat dilation and erosion of grayscale images are constructed based on NEQR. Then, the circuit realization of morphological gradient for grayscale images has been designed.

According to the characteristic of operations of the classical flat grayscale morphology, the quantum circuit realization mainly are divided into three steps: (1) Obtain the quantum image sets of neighborhood window pixels based on the shape of structuring element using a sequence of  $UA_1(n)$ ,  $US_1(n)$ , and  $U_C$  modules; (2) Finding the local-maximum and local-minimum through a series of QCOL and QCOS modules; (3) Using the PS module to subtract the local-minimum from the local-maximum.

Due to the unique advantages of parallel computing, entanglement, superposition, quantum computer brings bright prospect. Therefore, the quantum versions of erosion and dilation algorithms have been studied, the complexity of which is greatly reduced. Our future work will focus on the application of quantum morphology, such as quantum edge detection, noise reduction, feature detection, and image recognition.

**Acknowledgements** This work is supported by the National Natural Science Foundation of China under Grant Nos. 61763014, 61463016, 61462026, and 61762012, the National Key R\&D Plan under Grant No. 2018YFC1200200 and 2018YFC1200205, the Fund for Distinguished Young Scholars of Jiangxi Province under Grant No. 2018ACB21013, Science and technology research project of Jiangxi Provincial Education Department under Grant No. GJJ170382, Project of International Cooperation and Exchanges of Jiangxi Province under Grant No. 20161BBH80034, Project of Humanities and Social Sciences in colleges and universities of Jiangxi Province under Grant No. JC161023.

## References

1. Feynman, R.P.: Simulating physics with computers. *Int. J. Theor. Phys.* **21**(6/7), 467–488 (1982)
2. Yan, F., Ilyasu, A.M., Le, P., Q.: Quantum image processing: A review of advances in its security technologies. *International Int. J. Quantum. Inf.* **15**(3), 1730001 (2017)
3. Yan, F., Ilyasu, A.M., Venegas-Andraca, S.E.: A survey of quantum image representations. *Quantum Inf Process.* **15**(1), 1–35 (2016)
4. Vlasov, A.Y.: Quantum computations and images recognition. arXiv preprint quant-ph/9703010 (1997)
5. Schützhold, R.: Pattern recognition on a quantum computer. *Phys. Rev. A.* **67**(6), 062311 (2002)
6. Beach, G., Lomont, C., Cohen, C.: Quantum image processing (QuIP)[C]// applied imagery pattern recognition workshop. *Proceedings. IEEE.* **2004**, 39–44 (2003)
7. Deutsch, D.: Quantum theory, the Church-Turing principle and the universal quantum computer. *Pro. Roy. Soc. Lond. A: Math. Phys. Eng. Sci.* pp. 97–117 (1985)
8. Shor, P.: Algorithms for quantum computation: discrete logarithms and factoring. In: *Proceedings of the 35th Annual Symposium on Foundations of Computer Science.* 124–134 (1994)

9. Grover, L.: A fast quantum mechanical algorithm for database search. In: Proceedings of the 28th Annual ACM Symposium on Theory of Computing. 212–219(1996)
10. Iliyasu, A.M.: Towards the realisation of secure and efficient image and video processing applications on quantum computers. *Entropy*. **15**, 2874–2974 (2013)
11. Iliyasu, A. M.: Algorithmic Frameworks to support the Realisation of Secure and Efficient Image-Video Processing Applications on Quantum Computers. Ph.D. (Dr Eng.) Thesis, Tokyo Institute of Technology, Tokyo, Japan. 25 Sept. 2012
12. Iliyasu, A.M., Le, P.Q., Yan, F., et al.: A two-tier scheme for Greyscale Quantum Image Watermarking and Recovery. *Int. J. Innov Comput Appl*. **5**(2), 85–101 (2013)
13. Venegas-Andraca, S., Bose, S.: Storing, processing, and retrieving an image using quantum mechanics. *Proc. SPIE 5105 Quantum Inf. Compu*. **5105**(8), 134–147 (2003)
14. Venegas-Andraca, S., Ball, J.: Processing images in entangled quantum systems. *Quantum Inf. Process*. **9**(1), 1–11 (2010)
15. Latorre, J.: Image Compression and Entanglement. arXiv:quant-ph/0510031 (2005)
16. Le, P., Dong, F., Hirota, K.: A flexible representation of quantum images for polynomial preparation, image compression, and processing operations. *Quantum Inf. Process*. **10**(1), 63–84 (2011)
17. Zhang, Y., Lu, K., Gao, Y., Mao, W.: NEQR: a novel enhanced quantum representation of digital images. *Quantum Inf. Process*. **12**(8), 2833–2860 (2013)
18. Li, H.S., Zhu, Q., Zhou, R.G., et al.: Multi-dimensional color image storage and retrieval for a normal arbitrary quantum superposition state. *Quantum Inf Process*. **13**(4), 991–1011 (2014)
19. Li, H.S., Zhu, Q., Zhou, R.G., et al.: Multidimensional color image storage, retrieval, and compression based on quantum amplitudes and phases. *Inf Sci*. **273**(3), 212–232 (2014)
20. Li, H.S., Fan, P., Xia, H.Y., et al. Quantum Implementation Circuits of Quantum Signal Representation and Type Conversion. *IEEE Trans Circuits Syst I: Reg Papers*, (99):1–14 (2018)
21. Le, P. Q., Iliyasu, A.M., Dong, F., et al.: Fast geometric transformations on quantum images. *Iaeng Int J Appl Math*. **40**(3), (2010)
22. Fan, P., Zhou, R., Jing, N., Li, H.: Geometric transformations of multidimensional color images based on NASS. *Inf. Sci*. **340–341**, 191–208 (2016)
23. Wang, J., Jiang, N., Wang, L.: Quantum image translation. *Quantum Inf. Process*. **14**(5), 1589–1604 (2015)
24. Zhou, R.G., Tan, C., Hou, I.: Global and local translation designs of quantum image based on FRQI. *Int J Theor Phys*. **56**(4), 1382–1398 (2017)
25. Jiang, N., Wang, L.: Quantum image scaling using nearest neighbor interpolation. *Quantum Inf. Process*. **14**(5), 1559–1571 (2015)
26. Sang, J., Wang, S., Niu, X.: Quantum realization of the nearest-neighbor interpolation method for FRQI and NEQR. *Quantum Inf. Process*. **15**(1), 37–64 (2016)
27. Zhou, R.G., Hu, W., Fan, P., Hou, I.: Quantum realization of the bilinear interpolation method for NEQR. *Scientific Reports*. (7), 2511 (2017)
28. Zhou, R.G., Tan, C., Fan, P.: Quantum multidimensional color image scaling using nearest-neighbor interpolation based on the extension of FRQI. *Mod. Phys. Lett. B*. **31**(17), 1750184 (2017)
29. Zhou, R.G., Hu, W.W., Luo, G.F., et al.: Quantum realization of the nearest neighbor value interpolation method for INEQR. *Quantum Inf. Process*. **17**(7), 166 (2018)
30. Jiang, N., Wu, W.Y., Wang, L.: The quantum realization of Arnold and Fibonacci image scrambling. *Quantum Inf. Process*. **13**(5), 1223–1236 (2014)
31. Jiang, N., Wang, L., Wu, W.Y.: Quantum Hilbert image scrambling. *Int J Theor Phys*. **53**(7), 2463–2484 (2014)
32. Zhou, R.G., Shun, Y.J., Fan, P.: Quantum image Gray-code and bit-plane scrambling. *Quantum Inf. Process*. **14**(5), 1717–1734 (2015)
33. Mogos, G.: Hiding data in a QImage file. *Lecture Notes Eng. Compu. Sci*. **2174**(1), 448–452 (2009)
34. Iliyasu, A.M., Le, P.Q., Dong, F., et al.: Watermarking and authentication of quantum images based on restricted geometric transformations. *Information Sciences*. **186**(1), 126–149 (2012)
35. Zhang, W., Gao, F., Liu, B., et al.: A watermark strategy for quantum images based on quantum Fourier transform. *Quantum Inf. Process*. **12**(2), 793–803 (2013)
36. Song, X., Wang, S., El-Latif, A., et al.: Dynamic watermarking scheme for quantum images based on Hadamard transform. *Multimedia Systems*. **20**(4), 379–388 (2014)
37. Miyake, S., Nakamael, K.: A quantum watermarking scheme using simple and small-scale quantum circuits. *Quantum Inf. Process*. **15**(5), 1849–1864 (2016)
38. Jiang, N., Zhao, N., Wang, L.: LSB based quantum image steganography algorithm. *International J Theor Phys*. **55**(1), 107–123 (2016)
39. Heidari, S., Naseri, M.: A novel LSB based quantum watermarking. *Int J Theor Phys*. **55**(10), 1–14 (2016)

40. Zhou, R.G., Shun, Y.J.: Novel morphological operations for quantum image. *J Comput Inf Syst.* **11**(9), 3105–3112 (2015)
41. Zhou, R.G., Chang, Z., Fan, P., et al.: Quantum image morphology processing based on quantum set operation. *Int J Theor Phys.* **54**(6), 1974–1986 (2015)
42. Yuan, S., Mao, X., Li, T., et al.: Quantum morphology operations based on quantum representation model. *Quantum Inf. Process.* **14**(5), 1625–1645 (2015)
43. Fu, X., Ding, M., Sun, Y., et al.: A new quantum edge detection algorithm for medical images. *Proc SPIE Int Soc Opt Eng.* **7497**(9), 749724–749724-7 (2009)
44. Zhang, Y., Lu, K., Gao, Y.H.: QSobel: A novel quantum image edge extraction algorithm. *Science China Information Sciences.* **58**(1), 1–13 (2015)
45. Zhang, Y., Lu, K., Xu, K., et al.: Local feature point extraction for quantum images. *Quantum Inf. Processing.* **14**(5), 1573–1588 (2015)
46. Jiang, N., Dang, Y., Wang, J.: Quantum image matching. *Quantum Inf Process.* **15**(9), 3543–3572 (2016)
47. Barenco, A., Bennett, C.H., et al.: Elementary gates for quantum computation. *Phys Rev A At Mol Opt Phys.* **52**(5), 3457–3488 (1995)
48. Feynman, R.: Quantum mechanical computers. *Found. Phys.* **16**(6):507–531 (1986)
49. Toffoli, T.: Reversible computing. *Int. Col. Aut. Lan. Prog.* Springer, Berlin, Heidelberg (1980)
50. Peres, A.: Reversible logic and quantum computers. *Phys. Rev. A, Gen. Phys.* **32**(32), 3266–3276 (1985)
51. Thapliyal, H., Ranganathan, N.: Design of efficient reversible binary subtractors based on a new reversible gate. *IEEE Compu. Soc. Symp. VLSI.* 229–234 (2009)
52. Gonzalez, R.C., Wood, R.E.: *Digital Image Processing*, 2nd edn. Prentice Hall, Englewood Cliffs (2002)
53. Thapliyal H., Ranganathan N. A new design of the reversible subtractor circuit. *IEEE Conf. NANO.* 1430–1435 (2011)
54. Xu, X., Xiao, F., et al.: Application of dichotomy in decomposition of multi-line quantum logic gate. *J. Southeast Uni.* **40**(5), 928–931 (2010)